BIOCHEMISTRY
including biophysical chemistry & molecular biology

Article

pubs.acs.org/biochemistry

Dynamic Nuclear Polarization Study of Inhibitor Binding to the $M2_{18-60}$ Proton Transporter from Influenza A

Loren B. Andreas,[†] Alexander B. Barnes,[†] Björn Corzilius,[†] James J. Chou,[‡] Eric A. Miller,[†] Marc Caporini,[§] Melanie Rosay,[§] and Robert G. Griffin*[,†]

[†]Francis Bitter Magnet Laboratory and Department of Chemistry, Massachusetts Institute of Technology, Cambridge, Massachusetts 02139, United States

[‡]Department of Biological Chemistry and Molecular Pharmacology, Harvard Medical School, Boston, Massachusetts 02115, United States

[§]Bruker BioSpin Corporation, 15 Fortune Drive, Billerica, Massachusetts 01821, United States

Supporting Information

ABSTRACT: We demonstrate the use of dynamic nuclear polarization (DNP) to elucidate ligand binding to a membrane protein using dipolar recoupling magic angle spinning (MAS) NMR. In particular, we detect drug binding in the proton transporter $M2_{18-60}$ from influenza A using recoupling experiments at room temperature and with cryogenic DNP. The results indicate that the pore binding site of rimantadine is correlated with previously reported widespread chemical shift changes, suggesting functional binding in the pore. Futhermore, the ^{15}N-labeled ammonium of rimantadine was observed near A30 $^{13}C\beta$ and G34 $^{13}C\alpha$, suggesting a possible hydrogen bond to A30 carbonyl. Cryogenic DNP was required to observe the weaker external binding site(s) in a ZF-TEDOR spectrum. This approach is generally applicable, particularly for weakly bound ligands, in which case the application of MAS NMR dipolar recoupling requires the low temperatures to quench dynamic exchange processes. For the fully protonated samples investigated, we observed DNP signal enhancements of ∼10 at 400 MHz using only 4−6 mM of the polarizing agent TOTAPOL. At 600 MHz and with DNP, we measured a distance between the drug and the protein to a precision of 0.2 Å.

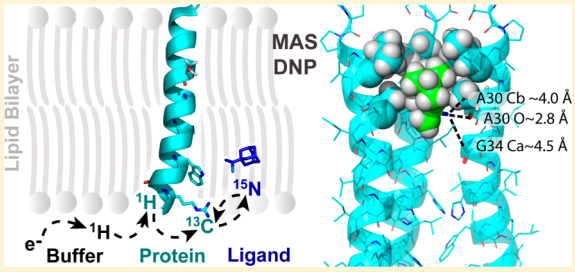

Magic angle spinning (MAS) NMR is a powerful analytical technique well suited for dynamic and structural characterization of membrane proteins and amyloid fibrils at atomic resolution.[1−3] In contrast with solution NMR, the ability to investigate systems of larger molecular mass without an inherent broadening of resonances is a major advantage of MAS NMR. However, the decreased molecular site concentration of larger molecules and detection of smaller magnetic moments of ^{13}C and ^{15}N spins means that sensitivity limits the application of traditional MAS NMR experiments. Dynamic nuclear polarization (DNP) can greatly increase the sensitivity of NMR by transferring the substantially higher polarization found in the electron spin reservoir to nuclear spins. DNP was first demonstrated at a magnetic field of 3.03 mT using a static sample of a metal;[4] these seminal studies also experimentally verified the Overhauser effect as an efficient polarization transfer mechanism. In the 1980s, DNP experiments performed on dielectric solids were integrated with MAS at 1.2 T, a low magnetic field by current standards.[5−8] The extension of DNP to magnetic field strengths used in contemporary NMR (≥5 T) has been achieved with the implementation of gyrotron oscillators as microwave power sources. Additional advances in NMR probe technology and development of stable organic radicals serving as the source of electron polarization have stimulated more widespread adoption of the approach and recently sparked considerable interest in the biological solid-state NMR community. DNP in conjunction with MAS NMR has now been proven to yield considerable gains in sensitivity, making possible a 25−10000-fold reduction in experiment time in studies of membrane proteins, amyloid fibrils, and peptide nanocrystals at 9 T.[9,10] Cryogenic MAS studies with improved probe technology on crystalline peptides demonstrated that resolution need not be compromised at low temperature.[11,12] MAS-DNP experiments on bacteriorhodopsin, a helical 7 transmembrane protein, have exploited both the sensitivity available from DNP as well as the cryogenic temperatures employed in such experiments to trap intermediates of its proton pumping cycle to better characterize the mechanism of ion translocation.[13,14] Experiments on the amyloid protein PI3-SH3 have shown that additional cross-peaks appear at low temperatures due to changes in protein dynamics, and the DNP-enhanced spectra were useful in determining details of the fibril structure.[15] In some, but not all cases, the cryogenic sample temperature leads to inhomogeneous line broadening and reduced resolution. Therefore, application of DNP to

Received: November 8, 2012
Revised: March 11, 2013
Published: March 12, 2013

biological systems of broad interest typically relies on well-resolved chemical shifts from spins found in unique chemical environments, or specific isotopic labeling of a cofactor, inhibitor, or residues to generate site-specific resolution. With the present state of the art and fields of about 9−14 T, successful application will likely involve carefully labeling the protein and ligand to make use of spectra with approximately 1.5 (^{13}C) and 3 (^{15}N) ppm line widths.[11,16]

In this study, we demonstrate that DNP can be used to elucidate ligand−protein interactions even in the weak (mM) binding regime using the proton transporter $M2_{18-60}$ from Influenza A virus and the inhibitor rimantadine. We present direct measurement of membrane protein−ligand interaction using MAS dipolar recoupling and DNP to detect the sites of drug binding in the tetrameric proton channel $M2_{18-60}$ in the nonconducting, high-pH state. This method is generally applicable to the study of drug or ligand binding, particularly for weak binding because general application of MAS NMR dipolar recoupling techniques to weak binding ligands requires the temperature to be lowered in order to quench dynamic exchange processes.[17] Although we stress the importance of low temperatures to quench exchange processes, binding sites can be detected while undergoing exchange using NOE measurements or dephasing experiments in which the exchange term commutes with the Hamiltonian. However, experiments such as ZF-TEDOR[18,19] that rely on transverse mixing do not commute with exchange terms and are made accessible by the low temperatures and DNP.

The M2 proton channel from influenza A is inhibited by the antiviral drugs rimantadine (Rmt) and amantadine (Amt). The full protein is 97 amino acids, and a construct comprising residues 21−61 has been shown to retain proton conductivity and inhibition by Amt and Rmt.[20] This construct and a similar 18−60 construct contain a single pass transmembrane helix and an amphipathic helix, which has been shown to stabilize the tetrameric assembly. An even shorter construct, $M2_{22-46}$, comprising the transmembrane segment, shows reduced inhibition by drug but remains drug sensitive. A controversy regarding the site of pharmacological inhibition arose from the observation of two different binding sites in various constructs of M2. Prevalence of *n*-terminal resistance mutations[21] and drug-induced changes in the pK_a of H37[22] suggested binding in the pore of the channel. However, structural studies showed multiple binding sites. An external site near D44 and R45 was observed by NOE in a solution NMR structure[23] of $M2_{18-60}$. On the other hand, an internal site in the pore near residues V27, S31, and G34A was proposed in a 3.5 Å diffraction structure of $M2_{22-46}$ at pH 5.3[24] and also observed in REDOR recoupling experiments.[25] When the drug was first detected in the pore of $M2_{22-46}$ in lipid bilayers, it was unclear if the conflicting results were due to truncating the protein near the external site, the particular micelle environment of the solution NMR structure, or other differences in sample preparations. The drug has now been shown to bind to the pore of $M2_{21-61}$,[26] ruling out problems with protein truncation. It is therefore known that the aminoadamantyl inhibitors Amt and Rmt bind to the pore of fully functional constructs in lipids, and the lack of pore NOE measurements in the solution NMR is likely due to the specific sample environment.

Nevertheless, since the drug has been shown to bind to both sites, the important remaining question was to definitively determine the site(s) responsible for inhibition. The pharmacological significance of each binding site has been supported based on resistance mutations and binding affinities, however there is not yet consensus regarding interpretation of the functional data.[27,28] Perhaps the strongest support for functional pore binding came from an interesting drug-sensitive chimera protein containing C-terminal residues from influenza B M2 and thus lacking the external binding site.[29] A recent study using this AM2-BM2 chimera solved a detailed structure of the tetramer with Rmt bound inside the pore.[30]

Given the existing evidence for multiple binding sites, most likely of differing affinity, we investigated $M2_{18-60}$ in lipid bilayers to explore the benefits of cryogenic DNP and to determine the locations of the functionally important drug amine group when bound to the protein. We present direct measurement of the drug in both binding sites and correlate pore binding with widespread chemical shift changes that have been interpreted as an indicator of structural rearrangement and functional binding.[17,31]

We used both wild-type (WT) M2 and the D21G, D24G double mutant to study drug binding. The use of the double mutant is justified by noting that the mutations occur outside the lipid embedded channel region. In addition, the mutant shows proton conduction and inhibition similar to the WT protein in liposome assays (see Figure S2 in the Supporting Information). Additionally, in all samples, cysteins 19 and 50 were changed to serine with no loss of function[27] in order to prevent uncontrolled disulfide bond formation. The two mutations from D to G remove ambiguity in potential cross-peaks arising from D44 in the external binding site. Thus, the WT_{18-60} sequence used in this work is RSNDSSDPLVVAAS-IIGILHLILWILDRLFFKSIYRFFEHGLK.

METHODS

The DNP-Enhanced ZF-TEDOR Experiment. In our DNP-enhanced ZF-TEDOR experiment, spin polarization is transferred several times before final detection. First, electron polarization on biradicals[32] such as TOTAPOL[33] is transferred to nearby protons via the cross effect[34] under the application of CW microwave irradiation and concurrently transferred to more distant protons via spin diffusion. The microwave irradiation frequency is set to 28.0498 GHz/T to maximize DNP efficiency using TOTAPOL. Next, ^{1}H polarization is transferred to ^{13}C in a cross-polarization step. The previous steps serve to increase the initial ^{13}C polarization and increase the sensitivity of the experiment. Finally, ZF-TEDOR recoupling[18] is used to transfer carbon polarization to ^{13}C−^{15}N two-spin order, the nitrogen chemical shift is encoded, and the two-spin order is reconverted into ^{13}C single quantum coherence for direct detection. It is in this final ZF-TEDOR step that the interaction between ^{13}C-labeled protein and ^{15}N-labeled drug is observed.

Optimization of Radical Concentration. A low concentration of 4 mM TOTAPOL was used in order to ensure that the radical induced only minimal paramagnetic relaxation effects on the protein. Particularly, reduction in transverse relaxation during long mixing periods could reduce signal intensity. Average carbonyl ^{13}C T_2 relaxation times of only ∼2 ms were found in a 40 mM TOTAPOL M2 sample with DNP enhancements of 26. A T_2 of 13−14 ms was found using 4 mM, similar to the T_2 value at 278 K. These effects are particularly pronounced in this relatively small protein and appear to be much less significant in previous studies that used 40 mM TOTAPOL to probe details of the active site of bacteriorhodopsin, which is shielded from close approach of radical by

the larger (26 kDa) protein.[11] General optimization of radical concentration for DNP is the subject of ongoing discussion.

M2 Sample Preparation. Pure $M2_{18-60}$ peptide was prepared by expression in *E. coli* as a fusion protein to TrpLe with a His 9 tag and purified with a nickel affinity column followed by chemical cleavage with cyanogen bromide in 70% formic acid and final purification on a C4 reverse phase HPLC column.[23,31] The Udorn strain of influenza was chosen, but with C19S and C50S mutations to prevent unwanted disulfide bond formation. Indicated samples additionally contained the D21G and D24G mutations.

M2 samples were prepared for MAS NMR as described previously[31] with modification to cryoprotect the sample in a glassy matrix[35,36] containing TOTAPOL for DNP. DPhPC lipid (Avanti Polar Lipids) and lyophilized $M2_{18-60}$ were dissolved in denaturing buffer (6 M guanidine, 40 mM phosphate, 30 mM glutamate, 3 mM sodium azide, pH 7.8, ≥33 mg/mL octyl glucoside (OG) detergent) with a lipid to protein ratio of 2:1 by weight. Buffer components were purchased from Sigma, and detergent was from Affymetrix. The resulting solution was then dialyzed in a 3.5 kDa cutoff dialysis cassette (Thermo) against 1 L of sample buffer (40 mM phosphate, 30 mM glutamate, 3 mM sodium azide, pH 7.8) for 7 days with 2 dialysis buffer changes per day. Lipid/M2 bilayers formed a white precipitate after ∼24 h. Solid material was pelleted by centrifugation at ∼100000*g* in a Beckmann ultracentrifuge. For pore-bound samples, a 4-fold molar excess of ^{15}N Rmt was added directly to the membrane pellet and incubated for 2 days at room temperature (∼22 °C). The pellet was then mixed with 2 mL of DNP buffer (60:40 by volume glycerol-d_8:75% deuterated sample buffer and 4 mM TOTAPOL[33]) and separated by centrifugation at 450000*g* for 12 h. DNP buffer was drained from below the sample, and the sample was packed in a 4 mm (Revolution NMR) or 3.2 mm (Bruker) sapphire MAS rotor. For pore-unbound samples, the membrane pellet was first mixed with DNP buffer and centrifuged at 450000*g*. A 4-fold molar excess of ^{15}N Rmt was then added to the sample immediately before packing into a sapphire MAS rotor.

NMR, Hardware, Referencing, and Processing. Standard NMR spectra were recorded using Cambridge Instruments spectrometers (courtesy of D. J. Ruben) operating at 500, 700, and 750 MHz ^{1}H frequencies and using triple-channel Varian 4 mm (500 MHz), Varian 3.2 mm (700 MHz), and Bruker 3.2 mm e-free (750 MHz) probes. DNP NMR spectra were acquired at 211 MHz using a Cambridge Instruments spectrometer and triple channel HCN probe equipped with a 4 mm MAS stator and waveguide for delivery of microwave irradiation from a gyrotron oscillator at 139.66 GHz.[37] Additional DNP spectra were recorded using commercial DNP spectrometers at 1H frequencies of 400[38] and 600 MHz (Bruker, Billerica, MA).

Chemical shifts were referenced using the published shifts of adamantane relative to DSS for ^{13}C referencing[39] and the IUPAC relative frequency ratios between DSS (^{13}C) and liquid ammonia (^{15}N)[40,41] for ^{15}N referencing. DNP spectra were referenced using the known chemical shifts of G34 at 278 K. Additional experimental details such as pulse sequences, NMR field strengths, and spinning frequencies are indicated in the figure captions. Spectra were processed using the NMRPipe[42] software package and visualized and assigned using Sparky (Goddard and Kneller, University of California, San Francisco). Spectra collected at 600 MHz were processed with 150 Hz Gaussian apodization in both ^{13}C and ^{15}N dimensions to improve the signal-to-noise ratio of the buildup curve. All other TEDOR spectra were processed with a 100 Hz Gaussian apodization window in the ^{13}C dimension and 150 Hz (crogenic DNP) and 30 Hz (278 K) in the ^{15}N dimension to improve sensitivity. Spectra in Figure 1 were processed with 30 Hz of Gaussian apodization. TPPM[43] decoupling field strengths of ∼100 kHz were used during TEDOR mixing periods, and either 100 or 83 kHz was used during acquisition. Power levels of 50−83 kHz were used for ^{13}C pulses and 20−40 kHz for ^{15}N pulses. Further details of the pulse sequences are provided in the Supporting Information.

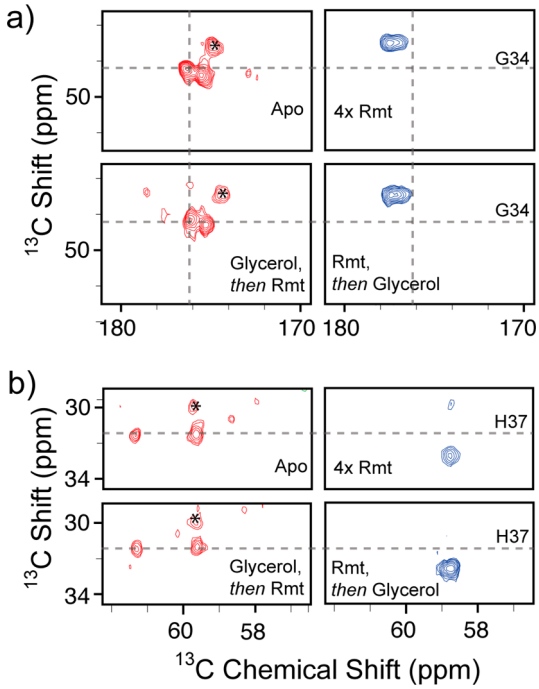

Figure 1. PDSD spectra of M2 acquired under four sample conditions show that chemical shifts are unperturbed by 60% glycerol if glycerol is the last component added to the sample. In (a) and (b) are shown cross-peaks of G34 and H37, respectively, in uniformly ^{13}C-labeled samples. The first three panels were recorded using a 700 MHz instrument with a Varian 3.2 mm triple channel probe spinning at 12.5 kHz. The fourth panel (4× Rmt *then* 60% glycerol) was recorded at 750 MHz with a triple channel Bruker e-free probe spinning at 13.4 kHz. These spectra of the D21G and D24G double mutant were recorded at ∼278 K using 15 ms of mixing. Peaks of G34 and H37 are displayed because of the excellent resolution in these regions of the spectrum and a clear change in frequency upon drug binding. Peaks other than those from G34 and H37 are indicated with an asterisk.

RESULTS

The DNP experiments are performed at low temperatures of ∼80−100 K where ice crystals would form from buffers commonly used for room temperature experiments. The samples are thus cryoprotected using 60 vol % glycerol. We show in Figure 1 that the chemical shifts are unperturbed by the addition of 60% glycerol, for both the apo and the functionally bound states at ∼278 K. The spectra provide a fingerprint that can be used to distinguish between apo M2 and functionally bound M2, where functional binding is determined by large chemical shift changes.[17,22,31] Previous reports found that addition of the aminoadamantyl drugs Rmt and Amt cause

dx.doi.org/10.1021/bi400150x | *Biochemistry* 2013, 52, 2774−2782

widespread chemical shift changes of up to several ppm to occur, and a functionally drug-bound spectrum is easily distinguished from an apo spectrum. On the basis of these fingerprint spectra, we conclude that the glycerol does not cause any significant change in these states of the protein. However, we find that glycerol increases the energy barrier for functional drug binding. In samples with drug added *before* glycerol, the drug-bound set of shifts was observed. In samples with drug added *after* glycerol, the apo set of peaks was observed. Since the final compositions of both samples are the same, we conclude that the difference is attributed to kinetically trapping the apo state and that the barrier for drug binding is increased by glycerol.

Spectra in Figure 1 were assigned using ZF-TEDOR[18,19] and PDSD[44,45] correlation experiments as was reported for WT_{18-60}[31] and by observation of only minor differences in chemical shift between WT_{18-60} and the D21G and D24G double mutant spectra of Figure 1. As with WT, we observe membrane embedded resonances from approximately residue 25 to 50 at 278 K. These observed residues span both proposed binding sites. Residue 24 appears weakly in some spectra, and residues 18−23 and 54−60 are not detected due to unfavorable mobility of this part of the protein. Spectra recorded at low temperature and with DNP were assigned based on the room temperature resonances for G34 and by using the observed range of chemical shifts reported in the BioMagResBank[46] for cross-peaks that do not show up at high temperature. These low-temperature cross-peaks could not be uniquely assigned; therefore, all possible assignments are indicated.

In order to observe a dipolar coupling between uniformly ^{13}C-labeled protein and ^{15}N-labeled inhibitor Rmt, we used a $^{13}C-^{15}N$ ZF-TEDOR experiment with 8.8 ms of mixing. Near room temperature (~278 K), the spectrum shows only two correlations to ^{15}N-labeled drug after 23 days of acquisition (Figure 2, red). In contrast, DNP-enhanced TEDOR spectra with 8.7 ms mixing at low (80−105 K) temperatures showed several additional cross-peaks (Figures 2 and 3, blue) and required only 2 days of acquisition due to the reduction in temperature and a signal enhancement factor of 11. Assignments consistent with the observed cross-peaks are indicated in the figures and clearly show that at room temperature the drug is observed in the pore near G34 and A30. The G34 cross-peak is unambiguously assigned at 278 K, based on the known unique resonances of G34 at this temperature. The A30 cross-peak is assigned by ruling out the only other alanine, A29, as a possible assignment because this residue is found on the outside of the channel far from G34, and the simplest interpretation of the data is that we are observing a single binding site in the pore.

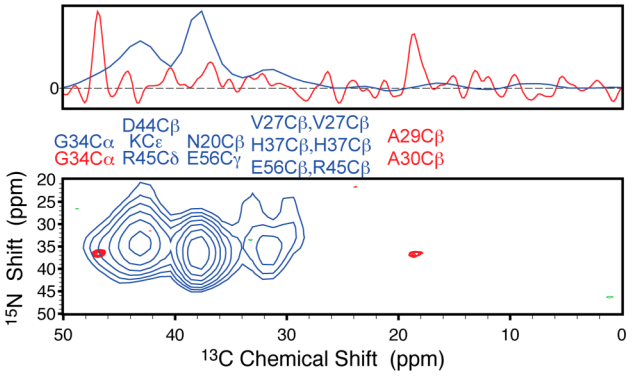

Figure 2. ZF-TEDOR spectra acquired at 278 K (red) show one set of cross-peaks, and those acquired at ~90 K using DNP (blue) show additional peaks. In red is shown an 8.8 ms TEDOR experiment acquired at 500 MHz and 10 kHz MAS with a sample temperature of 278 K. In blue is shown an 8.72 ms TEDOR experiment acquired at 211 MHz and 4.587 kHz MAS using DNP at 90 K. The 278 K spectrum was recorded in 23 days and the 90 K DNP spectrum in 2 days. Both spectra were acquired using the same sample of D21G−D24G M2 packed in a 4 mm sapphire rotor. ^{15}N-labeled Rmt was added before glycerol, and binding reached ~70% (as indicated by fingerprint spectra such as in Figure 1) before glycerol kinetically trapped the remaining 30% in the pore-unbound state. Possible assignments are indicated.

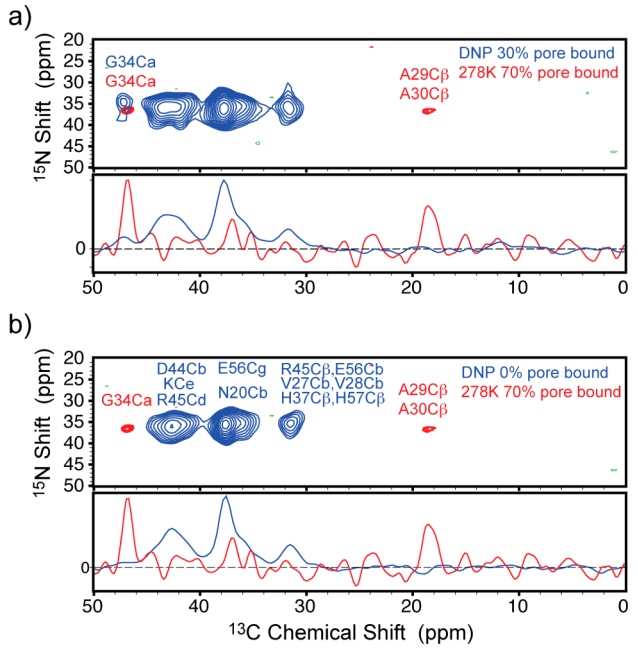

Figure 3. ZF-TEDOR spectra show that the pore binding site is correlated with chemical shift changes. A 400 MHz DNP-enhanced TEDOR spectrum (a) with 12.5 ms mixing is shown in blue. The wild-type M2 sequence was used, and ~30% of the sample was drug bound as indicated by chemical shifts. In (b), a similar spectrum is shown of D21G, D24G M2 but with the protein kinetically trapped in the apo state. Notably, the pore site at G34 is not detected in the functionally unbound sample shown in blue in (b). In red, the TEDOR spectrum acquired at ~278 K, 500 MHz, and 8.8 ms mixing of D21G, D24G M2 is presented for comparison. All possible assignments are listed for each peak in blue (DNP) and red (non-DNP).

At low temperature and using DNP, the drug is also observed on the periphery of the protein, consistent with the external site near D44 that was previously observed using solution NMR. In addition, cross-peaks are observed that are consistent with drug associating to E56 or N20, which may be another site of weak drug−protein association. The sample in Figure 2 was ~70% functionally bound before glycerol was added, and the remaining 30% was trapped in the apo state. The amount of functionally bound protein is less than 100% because it can take days for drug to penetrate and fully bind to the thick membrane pellet. Once glycerol is added, further binding is kinetically prevented. We used spectra similar to those shown in Figure 1 and the known chemical shifts of the apo and bound M2 to determine the extent of drug binding.

dx.doi.org/10.1021/bi400150x | *Biochemistry* 2013, 52, 2774−2782

In Figure 3, we show that if the protein is kinetically trapped in the apo state with drug present in the sample, the drug is observed only outside the pore. Isoleucine and leucine residues were ruled out as possible assignments by reverse labeling of these residue types with ^{12}C and observation of the same peaks (see Figure S1 in the Supporting Information).

The resolution of the DNP-enhanced spectrum at 211 MHz is significantly reduced compared to the 278 K spectrum acquired at 500 MHz, but the DNP-enhanced spectrum has much higher signal-to-noise, and the contours are displayed at a lower level. Therefore, the 2D spectra should not be used to infer resolution, and we include 1D slices below the 2D spectrum to show the inherent ^{13}C resolution in the spectra. We also see that the Ala Cβ resonance does not appear in the DNP spectrum. This is typical of $-CH_3$ groups at temperatures of ~100−200 K and results from 3-fold hopping at a rate that interferes with ^{1}H decoupling. Acquisition at temperatures where the methyl dynamics are much slower than the decoupling field results in a return of signal intensity, and ^{2}H labeling of the methyl group has a similar effect by reducing the couplings.[47]

In the 211 MHz DNP-enhanced spectrum (Figure 1), the G34Cα resonance is not resolved but appears as a shoulder on a larger nearby peak. In Figure 2a, we show a similar DNP spectrum, this time acquired at 400 MHz and applying 12.5 ms of mixing. The spectrum clearly shows a peak at G34Cα even though this sample had not equilibrated before addition of glycerol, and only ~1/3 of the sample showed drug binding as measured by the chemical shift changes. The spectrum in Figure 3b shows that when glycerol is added before the inhibitor, only the external binding site(s) are observed, once again indicating that the protein is trapped in the pore-unbound state by 60% glycerol. Pore binding is therefore correlated with chemical shift changes. Coupled with a recent report showing that the drug resistant S31N mutant of M2 does not exhibit chemical shift changes with the addition of Rmt,[48] the evidence points convincingly to the pore site as responsible for inhibition in agreement with recent reports.[26,30] Despite other glycines in the sequence of M2, the glycine cross-peaks in the DNP spectra can be uniquely assigned to the pore glycine, G34, because glycine peaks are missing from the spectrum when the protein is trapped in the pore-unbound state; the weaker association of the drug on the periphery of the channel does not result in detection of TEDOR cross-peaks to glycine Cαs.

With this unique ^{15}N Rmt to G34 Cα assignment under DNP conditions, we can proceed with standard MAS NMR experiments designed to measure internuclear distances. In Figure 4, we show the results of a ZF-TEDOR buildup curve recorded at 600 MHz with DNP using uniformly ^{13}C-labeled WT $M2_{18-60}$ in a sample with nearly saturated binding to the pore. The maximum signal-to-noise ratio in the DNP enhanced TEDOR experiment was 15 at 11.52 ms of mixing, which is sufficient to measure a distance using an analytical fitting procedure described previously.[18] The data are inconsistent with a drug amine centered in the channel, and the fit distance depends somewhat on whether the amine is near two or one helices. A fit of 4.3 or 4.0 ± 0.2 Å was found for fits with two and one G34 Cαs, respectively. Details of the fit are described below.

An overall scaling factor, λ, is used in the fit to account for an unknown cross-polarization intensity and experimental imperfections. Fortunately, we can reduce the number of free parameters in the fit by using the known distance associated

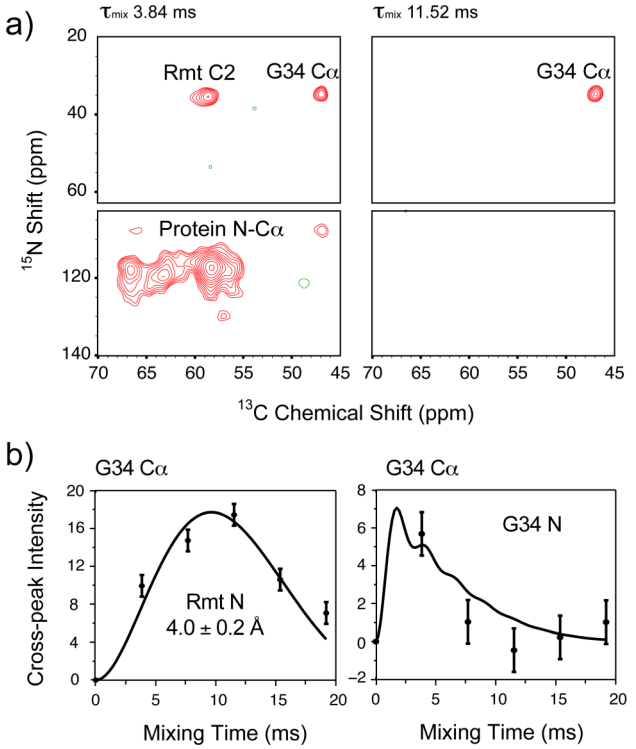

Figure 4. ZF-TEDOR spectra collected at 600 MHz with DNP are contoured at two mixing times in (a) and displayed for the G34 cross-peak as a function of mixing time in (b). At 3.84 ms mixing (a, left), one bond cross-peaks are detected due to the natural abundance of ~1% ^{13}C Rmt drug, and ~0.36% ^{15}N protein. By 11.52 ms (a, right), these natural abundance cross-peaks have decayed and only the cross-peak of interest remains. In (b), the G34 cross-peak intensity is shown as a function of mixing time (points ± the spectrum rms noise level), with the best-fit simulation as described in the text (smooth curve). The fit resulted in a distance of 4.0 ± 0.2 Å. The G34 N−Cα cross-peak was simultaneously fit (b, right) to reduce the degrees of freedom in the fit. A low natural abundance of ^{15}N (~0.36%) accounts for the reduced signal of this curve. The spectra were recorded in ~4 days at a spinning frequency of 12.5 kHz and a temperature of ~100 K. The DNP enhancement factor was 2.5.

with a 1-bond cross-peak from G34Cα to G34N to determine λ. A natural abundance of 0.36% for ^{15}N was used to scale this peak in the fit, and both the short distance of 1.5 Å and the long distance of interest were simulated simultaneously using the same value for λ. The fit parameter Γ_2 is an exponential relaxation term that is dominated by ^{13}C transverse relaxation and was therefore fit using one value for both curves. The average ^{13}C Γ_2 of the sample was determined to be above 100 s^{-1} using an echo experiment, justifying fitting over a range of Γ_2 values between 50 and 150 s^{-1}, as done for crystalline peptides.[18] The one bond J coupling of G34 was varied over a wide range of 40−60 Hz in the fit but influenced the fit distance by less than 0.1 Å. Typical values of $^{1}J_{C'-C\alpha}$ are about 55 Hz.[49] Two percent of the sample was assumed to have no J coupling based on an estimate of 98% enrichment of ^{13}C using 99% ^{13}C glucose and a ^{12}C starter culture. A Monte Carlo approach was used to estimate the measurement error by refitting 1000 times with the addition of the appropriate noise level of the spectrum[18] to each curve. The resulting distribution was used to calculate the rms deviation. All error estimates are reported at 1 rmsd.

dx.doi.org/10.1021/bi400150x | Biochemistry 2013, 52, 2774−2782

The final consideration in properly fitting the distance is to determine how many of the helices in the tetramer are close enough to contribute to the cross-peak. If we assume all four are equidistant from the drug amine, then a fit distance of 4.8 ± 0.2 Å is found. With the drug amine positioned between G34 Cα and A30 Cβ, this distance is incompatible with the solution constraints, which allow a minimum distance of about 5.5 Å, and certainly incompatible with the more loosely packed diffraction structures. If we fit the data with two G34 Cαs equidistant from the drug amine, and the other two at a reasonable distance of 6.5 Å or above, we determine a fit distance of 4.3 ± 0.2 Å. Finally, if we assume the ^{15}N interacts primarily with one helix, with the other G34 Cαs at reasonable distances of 5.5, 6.5, and 6.5 Å, the fit distance is 4.0 ± 0.2 Å. This fit is shown in Figure 4b.

In order to visualize the pore binding site for which we found unambiguous constraints, we have performed a simulated annealing using the program XPLOR-NIH.[50] In addition to the two new constraints from ZF-TEDOR at ∼278 K and with cryogenic DNP, we used structural constraints from a solution NMR structure[23] and a constraint based on previously reported ^{2}H−^{13}C REDOR experiments.[25,51] Based on the DNP enhanced buildup curve, an upper limit of 4.5 Å was allowed for the Rmt amine to G34 Cα. Similar constraints, entered in the calculation as 3.5 ± 1 Å, were entered for ^{15}N-Rmt to A30 Cβ based on the similar intensity of this cross-peak at room temperature. Constraints of 3.5 ± 1 Å were also applied between the V27 Cγ1 and Rmt CH_2 groups farthest from the amine in order to orient the adamantyl cage consistent with a recent report using the 22−46 construct.[51] Drug constraints were introduced to only one of the four strands of the protein. Given the symmetry of the channel, and the fact that we observe two sets of chemical shifts, the drug amine may hop between 2 or 4 of the helices and thus prevent breaking of the 2-fold symmetry of the channel. A representative result from the simulated annealing is shown in Figure 5.

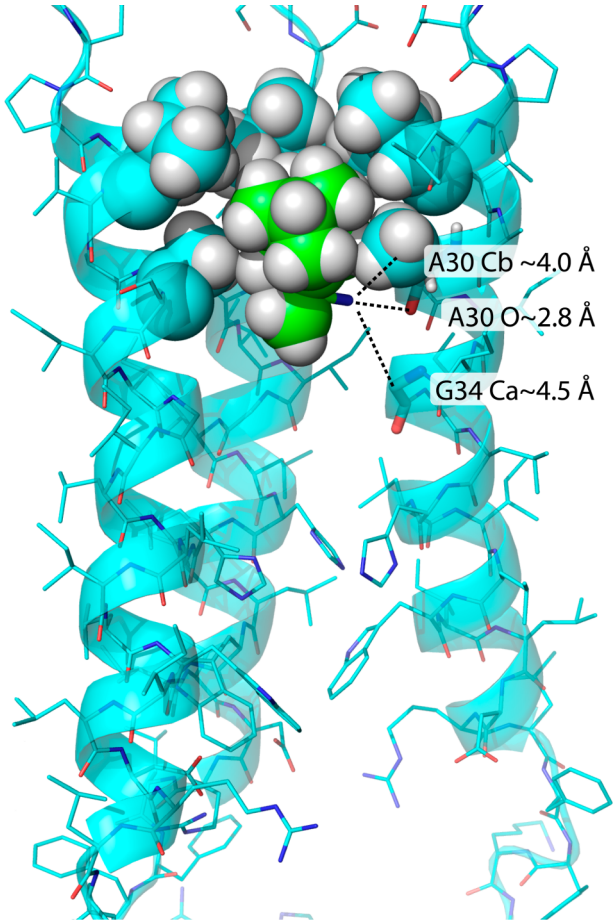

Figure 5. A structural model of the pore binding site is shown using distance constraints from DNP-enhanced TEDOR experiments, 278 K TEDOR experiments, and previously reported data. The structural model was calculated using XPLOR-NIH and converged to a set of similar structures with 0 violations. A representative structure is shown with drug in green and protein in blue. Three distances to the drug ^{15}N are shown, two of which (A30 Cβ and G34 Cα) are the result of TEDOR measurements. The third distance is a result of the structure calculation and suggests a possible hydrogen bond between the drug amine and the protein at A30 carbonyl oxygen. The constraints deposited in the protein data bank for the solution NMR structure 2RLF[24] were used to define the tetrameric assembly. Distance constraints of 3.5 ± 1 Å were introduced between the drug ^{15}N and A30 Cβ and between drug ^{15}N and G34Cα based on TEDOR spectra. Finally, constraints of 3.5 ± 1 Å were introduced between the V27 Cγ1 and Rmt CH_2 groups farthest from the amine in order to orient the adamantyl cage consistent with previous reports.

DISCUSSION

In previous experiments, two binding sites have been observed: a pore site in $M2_{22-46}$ and $M2_{22-62}$ and an external site in $M2_{18-60}$ and $M2_{22-46}$. We have confirmed the internal site in the $M2_{18-60}$ construct using DNP MAS at 100 K. Additionally, a drug−protein association is observed on the periphery of the channel, consistent with the external site; however, the location and affinity are not determined. The pore site was found to have a significantly higher barrier, causing the protein to be kinetically trapped near room temperature in the pore-unbound state using 60% glycerol. Pore-bound Rmt was observed in a standard ZF-TEDOR experiment at ∼278 K, indicating that the drug is exchanging with the free population slower than the millisecond time scale. In contrast, the external association was only observed at the low temperatures used in DNP experiments, indicating that drug exchange likely results in loss of signal at 278 K. The external site is observed even when the protein has been kinetically trapped in the pore-unbound state (as determined by chemical shift changes), indicating that this site has a low barrier, is not responsible for chemical shift changes, and is most likely not responsible for pharmacological binding.

Measurements of the external binding site(s) of the protein appear to have some specificity even though they are not unambiguously assigned. For example, we see a cross-peak to E56 or N20, but not to neighboring H57 and G58, or S19, S22, and S23 residues. A completely nonspecific interaction should result in some detection of these external glycine and serine residues. Still, partitioning of the drug into the interfacial region of the membrane may significantly enhance population of these sites. Whether the observation of specificity at these weaker sites requires a slow cooling rate and annealing of the protein remains an open to further investigation.

Although binding to the pore of the channel has been observed previously, the present work is the first to our knowledge to directly determine the position of the drug amine group between residues 30 and 34. A previous report in bilayers determined the correct orientation of the drug in the channel but placed the amine group about a half helical turn toward the carboxy terminus of the protein compared to our measure-

dx.doi.org/10.1021/bi400150x | Biochemistry 2013, 52, 2774−2782

ments.[51] Additionally, our data suggest a hydrogen bond between the drug amine and the A30 carbonyl. Out of 30 calculated structures that did not violate any of the constraints, the distance between the drug amine nitrogen and the A30 carbonyl oxygen was found to vary between 2.4 and 3.5 Å, suggesting a hydrogen bond between drug and protein at this location. Though this agrees with a previously observed conformational heterogeneity at A30s hydrogen bonding donor G34 among drug bound and apo samples,[52] and with a recent solution NMR structure of a chimera protein containing C-terminal residues from influenza-B M2,[30] it is the first time this specific interaction has been observed using WT protein.

The structural model presented here is consistent with previous measurements on the Rmt tilt angle in the pore of $M2_{22-46}$[51] determined using measurements of the scaled ^2H quadrupole splitting of ^2H-labeled Rmt. The amine was found to point toward the C-terminal end of the channel with a 13° angle between the bilayer normal and the adamantly group. Rmt is tilted by up to ~35° in the structural model shown in Figure 5, with most of the ensemble clustered within about 12°. A large distribution in the tilt angle is not surprising because we have not made measurements to determine this angle, with the adamantyl cage instead being positioned by steric crowding within the channel. Interestingly, the tilt angle of the related drug Amt was previously found to be a much larger 37°,[25] suggesting that the shorter link between the adamantyl group and the amine in Amt might force the adamatyl group to rotate so that both the amine and the adamantyl cage can occupy approximately the same locations in the channel for both drugs (see Figure S3 in the Supporting Information). The evidence for a drug−protein hydrogen bond at A30 carbonyl (both the tilt angle of Amt and the TEDOR measurements on Rmt) could help inform molecular dynamics simulations of this channel that have instead proposed hydrogen bonding to water and a small tilt angle[53] or even found the amine group pointing toward the nitrogen terminus of the protein.[54]

CONCLUSIONS

We have shown that DNP can be used with MAS for the identification of ligand−protein interactions. The low temperatures used for DNP quenches dynamic processes that interfere with dipolar recoupling experiments, particularly for weakly bound ligands. These effects were demonstrated in M2, in which the pore binding site is evident at 278 K, and weaker binding to the periphery of the protein is only observed at cryogenic temperatures. In addition, we found that glycerol can be used to kinetically prevent the drug from entering the pore, thereby allowing us to make samples with the pore unoccupied, but with drug bound to the external site. With these samples, we have correlated chemical shift changes with binding in the pore. In addition, we located the position of the functionally important drug amine group in relation to specific protein ^{13}C atoms, placing the amine close enough to A30 carbonyl to form a hydrogen bond. Further experiments could include BASE-TEDOR experiments[18] to improve precision of the distance measurements as well as unambiguous assignment experiments to precisely determine the external binding site(s).

ASSOCIATED CONTENT

Supporting Information

Additional spectra of reverse labeled M2 ruling out isoleucine and leucine cross-peaks; liposome assays showing drug sensitivity of M2 constructs; illustration of Rmt and Amt tilt angles; pulse sequences and spectroscopic details. This material is available free of charge via the Internet at http://pubs.acs.org.

AUTHOR INFORMATION

Corresponding Author

*E-mail rgg@mit.edu, Ph 617-253-5597.

Funding

This work was supported by NIH grants EB-001960, EB-002026, AI-067438, GM-094608, and EB-002804.

Notes

The authors declare no competing financial interest.

ACKNOWLEDGMENTS

We thank Rafal Pielak for help running the liposome assay and help with sample preparation. We thank Marvin Bayro and Galia Debelouchina for help with the DNP acquisition at Bruker Biospin, Remy Sounier, and Marcelo Berardi for helpful discussions regarding sample preparation. Matthew Eddy and Yongchao Su are gratefully acknowledged for help in testing TEDOR fitting code against a known system.

ABBREVIATIONS

CW, continuous wave; DNP, dynamic nuclear polarization; HPLC, high pressure liquid chromatography; MAS, magic angle spinning; NMR, nuclear magnetic resonance; Rmt, rimantadine; Amt, amantadine; ZF-TEDOR, *z*-filtered transferred echo double resonance; rms, root-mean-square; TPPM, two pulse phase modulation.

REFERENCES

(1) Ritter, C., Maddelein, M. L., Siemer, A. B., Lührs, T., Ernst, M., Meier, B. H., Saupe, S., and Riek, R. (2005) Correlation of Structure and Infectivity of the HET-s Prion. *Nature 435*, 844.

(2) Ahuja, S., Hornak, V., Yan, E. C. Y., Syrett, N., Goncalves, J. A., Hirshfeld, A., Ziliox, M., Sakmar, T. P., Sheves, M., and Reeves, P. J. (2009) Helix Movement Is Coupled to Displacement of the Second Extracellular Loop in Rhodopsin Activation. *Nat. Struct. Mol. Biol. 16*, 168−175.

(3) Hu, F., Luo, W., and Hong, M. (2010) Mechanisms of Proton Conduction and Gating in Influenza M2 Proton Channels from Solid-State NMR. *Science 330*, 505.

(4) Carver, T. R., and Slichter, C. P. (1953) Polarization of Nuclear Spins in metals. *Phys. Rev. 92*, 212−213.

(5) Afeworki, M., Mckay, R. A., and Schaefer, J. (1992) Selective Observation of the Interface of Heterogeneous Polycarbonate Polystyrene Blends by Dynamic Nuclear-Polarization C-13 NMR Spectroscopy. *Macromolecules 25*, 4084−4091.

(6) Afeworki, M., Vega, S., and Schaefer, J. (1992) Direct Electron-to-Carbon Polarization Transfer in Homgeneously-Doped Polycarbonates. *Macromolecules 25*, 4100−4106.

(7) Macho, V., Kendrick, R., and Yannoni, C. S. (1983) Cross Polarization Magic-Angle Spinning NMR at Cryogenic Temperatures. *J. Magn. Reson. 52*, 450−456.

(8) Wind, R. A., Anthonio, F. E., Duijvestijn, M. J., Smidt, J., Trommel, J., and Vette, G. M. C. d. (1983) Experimental Setup for Enhanced ^{13}C NMR Spectroscopy in Solids Using Dynamic Nuclear Polarization. *J. Magn. Reson. 52*, 424−434.

(9) Debelouchina, G., Bayro, M., van der Wel, P., Caporini, M., Barnes, A., Rosay, M., Maas, W., and Griffin, R. (2010) Dynamic Nuclear Polarization-Enhanced Solid-State NMR Spectroscopy of GNNQQNY Nanocrystals and Amyloid Fibrils. *Phys. Chem. Chem. Phys. 12*, 5911−5919.

(10) Bajaj, V. S., Mak-Jurkauskas, M. L., Belenky, M., Herzfeld, J., and Griffin, R. G. (2010) DNP Enhanced Frequency-Selective TEDOR Experiments in Bacteriorhodopsin. *J. Magn. Reson. 202*, 9−13.
(11) Barnes, A. B., Corzilius, B., Mak-Jurkauskas, M. L., Andreas, L. B., Bajaj, V. S., Matsuki, Y., Belenky, M., Lugtenburg, J., Sirigiri, J. R., Temkin, R. J., Herzfeld, J., and Griffin, R. G. (2010) Resolution and Polarization Distribution in Cryogenic DNP/MAS Experiments. *Phys. Chem. Chem. Phys. 12*, 5861−5867.
(12) Barnes, A. B., Mak-Jurkauskas, M. L., Matsuki, Y., Bajaj, V. S., van der Wel, P. C. A., DeRocher, R., Bryant, J., Sirigiri, J. R., Temkin, R. J., Lugtenburg, J., Herzfeld, J., and Griffin, R. G. (2009) Cryogenic Sample Exchange NMR probe for Magic Angle Spinning Dynamic Nuclear Polarization. *J. Magn. Reson. 198*, 261−270.
(13) Bajaj, V., Mak-Jurkauskas, M., Belenky, M., Herzfeld, J., and Griffin, R. (2009) Functional and Shunt States of Bacteriorhodopsin Resolved by 250 GHz Dynamic Nuclear Polarization Enhanced Solid-State NMR. *Proc. Natl. Acad. Sci. U. S. A. 106*, 9244.
(14) Mak-Jurkauskas, M. L., Bajaj, V. S., Hornstein, M. K., Belenky, M., Temkin, R. J., Griffin, R. G., and Herzfeld, J. (2008) Energy Transformations Early in the Bacteriorhodopsin Photocycle Revealed by DNP-Enhanced Solid State NMR. *Proc. Natl. Acad. Sci. U. S. A. 105*, 883−888.
(15) Bayro, M. J., Debelouchina, G. T., Eddy, M. T., Birkett, N. R., Macphee, C. E., Rosay, M., Maas, W. E., Dobson, C. M., and Griffin, R. G. (2011) Intermolecular Structure Determination of Amyloid Fibrils with Magic-Angle Spinning and Dynamic Nuclear Polarization NMR. *J. Am. Chem. Soc. 133*, 13967−13974.
(16) Rosay, M., Zeri, A. C., Astrof, N. S., Opella, S. J., Herzfeld, J., and Griffin, R. G. (2001) Sensitivity-Enhanced NMR of Biological Solids: Dynamic Nuclear Polarization of Y21M fd Bacteriophage and Purple Membrane. *J. Am. Chem. Soc. 123*, 1010−1011.
(17) Cady, S. D., and Hong, M. (2008) Amantadine-Induced Conformational and Dynamical Changes of the Influenza M2 Transmembrane Proton Channel. *Proc. Natl. Acad. Sci. U. S. A. 105*, 1483.
(18) Jaroniec, C. P., Filip, C., and Griffin, R. G. (2002) 3D TEDOR NMR Experiments for the Simultaneous Measurement of Multiple Carbon-Nitrogen Distances in Uniformly ^{13}C,^{15}N-Labeled Solids. *J. Am. Chem. Soc. 124*, 10728−10742.
(19) Hing, A. W., Vega, S., and Schaefer, J. (1992) Transferred-Echo Double-Resonance NMR. *J. Magn. Reson. 96*, 205−209.
(20) Ma, C., Polishchuk, A. L., Ohigashi, Y., Stouffer, A. L., Schon, A., Magavern, E., Jing, X., Lear, J. D., Freire, E., Lamb, R. A., DeGrado, W. F., and Pinto, L. H. (2009) Identification of the Functional Core of the Influenza A Virus A/M2 Proton-Selective Ion Channel. *Proc. Natl. Acad. Sci. U. S. A. 106*, 12283−12288.
(21) Holsinger, L. J., Nichani, D., Pinto, L. H., and Lamb, R. A. (1994) Influenza A Virus M2 Ion Channel Protein: A Structure-Function Analysis. *J. Virol. 68*, 1551−1563.
(22) Hu, J., Fu, R. Q., and Cross, T. A. (2007) The Chemical and Dynamical Influence of the Anti-Viral Drug Amantadine on the M-2 Proton Channel Transmembrane Domain. *Biophys. J. 93*, 276−283.
(23) Schnell, J., and Chou, J. (2008) Structure and Mechanism of the M2 Proton Channel of Influenza A Virus. *Nature 451*, 591−595.
(24) Stouffer, A. L., Acharya, R., Salom, D., Levine, A. S., Di Costanzo, L., Soto, C. S., Tereshko, V., Nanda, V., Stayrook, S., and DeGrado, W. F. (2008) Structural Basis for the Function and Inhibition of an Influenza Virus Proton Channel. *Nature 451*, 596−599.
(25) Cady, S. D., Schmidt-Rohr, K., Wang, J., Soto, C. S., DeGrado, W. F., and Hong, M. (2010) Structure of the Amantadine Binding Site of Influenza M2 Proton Channels in Lipid Bilayers. *Nature 463*, 689.
(26) Cady, S., Wang, T., and Hong, M. (2011) Membrane-Dependent Effects of a Cytoplasmic Helix on the Structure and Drug Binding of the Influenza Virus M2 Protein. *J. Am. Chem. Soc. 133*, 11572−11579.
(27) Pielak, R. M., Schnell, J. R., and Chou, J. J. (2009) Mechanism of Drug Inhibition and Drug Resistance of Influenza A M2 Channel. *Proc. Natl. Acad. Sci. U. S. A. 106*, 7379−7384.
(28) Jing, X., Ma, C., Ohigashi, Y., Oliveira, F. A., Jardetzky, T. S., Pinto, L. H., and Lamb, R. A. (2008) Functional Studies Indicate Amantadine Binds to the Pore of the Influenza A Virus M2 Proton-Selective Ion Channel. *Proc. Natl. Acad. Sci. U. S. A. 105*, 10967−10972.
(29) Ohigashi, Y., Ma, C., Jing, X., Balannick, V., Pinto, L. H., and Lamb, R. A. (2009) An Amantadine-Sensitive Chimeric BM2 Ion Channel of Influenza B Virus Has Implications for the Mechanism of Drug Inhibition. *Proc. Natl. Acad. Sci. U. S. A. 106*, 18775−18779.
(30) Pielak, R. M., Oxenoid, K., and Chou, J. J. (2011) Structural Investigation of Rimantadine Inhibition of the AM2-BM2 Chimera Channel of Influenza Viruses. *Structure 19*, 1655−1663.
(31) Andreas, L. B., Eddy, M. T., Pielak, R. M., Chou, J., and Griffin, R. G. (2010) Magic Angle Spinning NMR Investigation of Influenza A M2(18−60): Support for an Allosteric Mechanism of Inhibition. *J. Am. Chem. Soc. 132*, 10958−10960.
(32) Hu, K.-N., Yu, H.-h., Swager, T. M., and Griffin, R. G. (2004) Dynamic Nuclear Polarization with Biradicals. *J. Am. Chem. Soc. 126*, 10844−10845.
(33) Song, C., Hu, K. N., Joo, C. G., Swager, T. M., and Griffin, R. G. (2006) TOTAPOL: A Biradical Polarizing Agent for Dynamic Nuclear Polarization Experiments in Aqueous Media. *J. Am. Chem. Soc. 128*, 11385−11390.
(34) Wollan, D. S. (1976) Dynamic Nuclear Polarization with an Inhomogeneously Broadened ESR Line. I. Theory. *Phys. Rev. B 13*, 3671−3685.
(35) Rosay, M., Lansing, J. C., Haddad, K. C., Bachovchin, W. W., Herzfeld, J., Temkin, R. J., and Griffin, R. G. (2003) High Frequency Dynamic Nuclear Polarization in MAS Spectra of Membrane and Soluble Proteins. *J. Am. Chem. Soc. 125*, 13626−13627.
(36) Bajaj, V. S., Hornstein, M. K., Kreischer, K. E., Sirigiri, J. R., Woskov, P. P., Mak, M., Herzfeld, J., Temkin, R. J., and Griffin, R. G. (2007) 250 GHz Gyrotron for Dynamic Nuclear Polarization in Biological Solid State NMR. *J. Magn. Reson. 190*, 86−114.
(37) Joye, C. D., Griffin, R. G., Hornstein, M. K., Hu, K. N., Kreischer, K. E., Rosay, M., Shapiro, M. A., Sirigiri, J. R., Temkin, R. J., and Woskov, P. P. (2006) Operational Characteristics of a 14-W 140-GHz Gyrotron for Dynamic Nuclear Polarization. *IEEE Trans. Plasma Sci. IEEE Nucl. Plasma Sci. Soc. 34*, 518−523.
(38) Rosay, M., Tometich, L., Pawsey, S., Bader, R., Schauwecker, R., Blank, M., Borchard, P. M., Cauffman, S. R., Felch, K. L., and Weber, R. T. (2010) Solid-State Dynamic Nuclear Polarization at 263 GHz: Spectrometer Design and Experimental Results. *Phys. Chem. Chem. Phys. 12*, 5850−5860.
(39) Morcombe, C. R., and Zilm, K. W. (2003) Chemical Shift Referencing in MAS Solid State NMR. *J. Magn. Reson. 162*, 479−486.
(40) Markley, J. L., Bax, A., Arata, Y., Hilbers, C. W., Kaptein, R., Sykes, B. D., Wright, P. E., and Wuthrich, K. (1998) Recommendations for the Presentation of NMR Structures of Proteins and Nucleic Acids. IUPAC-IUBMB-IUPAB Inter-Union Task Group on the Standardization of Data Bases of Protein and Nucleic Acid Structures Determined by NMR Spectroscopy. *J. Biomol. NMR 12*, 1−23.
(41) Harris, R. K., Becker, E. D., Cabral de Menezes, S. M., Goodfellow, R., and Granger, P. (2002) NMR Nomenclature: Nuclear Spin Properties and Conventions for Chemical Shifts. IUPAC Recommendations 2001. *Solid State Nucl. Magn. Reson. 22*, 458−483.
(42) Delaglio, F., Grzesiek, S., Vuister, G. W., Zhu, G., Pfeifer, J., and Bax, A. (1995) NMRPipe: A Multidimensional Spectral Processing System Based on UNIX Pipes. *J. Biomol. NMR 6*, 277−293.
(43) Bennett, A. E., Rienstra, C. M., Auger, M., Lakshmi, K. V., and Griffin, R. G. (1995) Heteronuclear Decoupling in Rotating Solids. *J. Chem. Phys. 103*, 6951−6958.
(44) Szeverenyi, N. M., Sullivan, M. J., and Maciel, G. E. (1982) Observation of Spin Exchange by Two-Dimensional Fourier Transform ^{13}C Cross Polarization-Magic-Angle-Spinning. *J. Magn. Reson. 47*, 462−475.
(45) Szeverenyi, N. M., Bax, A., and Maciel, G. E. (1983) Proton-Exchange Rates in Solid Tropolone As Measured via ^{13}C CP/MAS NMR. *J. Am. Chem. Soc. 105*, 2579−2582.

(46) Ulrich, E. L., Akutsu, H., Doreleijers, J. F., Harano, Y., Ioannidis, Y. E., Lin, J., Livny, M., Mading, S., Maziuk, D., Miller, Z., Nakatani, E., Schulte, C. F., Tolmie, D. E., Kent Wenger, R., Yao, H., and Markley, J. L. (2008) BioMagResBank. *Nucleic Acids Res. 36*, D402−408.
(47) Maus, D. C., CopiÈ, V., Sun, B., Griffiths, J. M., Griffin, R. G., Luo, S., Schrock, R. R., Liu, A. H., Seidel, S. W., and Davis, W. M. (1996) A Solid-State NMR Study of Tungsten Methyl Group Dynamics in $[W(\eta^5\text{-}C_5Me_5)Me_4][PF_6]$. *J. Am. Chem. Soc. 118*, 5665−5671.
(48) Andreas, L. B., Eddy, M. T., Chou, J. J., and Griffin, R. G. (2012) Magic-Angle-Spinning NMR of the Drug Resistant S31N M2 Proton Transporter from Influenza A. *J. Am. Chem. Soc. 134*, 7215−7218.
(49) Chen, L., Kaiser, J. M., Lai, J., Polenova, T., Yang, J., Rienstra, C. M., and Mueller, L. J. (2007) J-Based 2D Homonuclear and Heteronuclear Correlation in Solid-State Proteins. *Magn. Reson. Chem. 45*, S84−S92.
(50) Schwieters, C. D., Kuszewski, J. J., Tjandra, N., and Clore, G. M. (2003) The Xplor-NIH NMR Molecular Structure Determination Package. *J. Magn. Reson. 160*, 65−73.
(51) Cady, S. D., Wang, J., Wu, Y., DeGrado, W. F., and Hong, M. (2011) Specific Binding of Adamantane Drugs and Direction of Their Polar Amines in the Pore of the influenza M2 Transmembrane Domain in Lipid Bilayers and Dodecylphosphocholine Micelles Determined by NMR Spectroscopy. *J. Am. Chem. Soc. 133*, 4274−4284.
(52) Yi, M., Cross, T. A., and Zhou, H. X. (2009) Conformational Heterogeneity of the M2 Proton Channel and a Structural Model for Channel Activation. *Proc. Natl. Acad. Sci. U. S. A. 106*, 13311−13316.
(53) Wang, J., Ma, C., Fiorin, G., Carnevale, V., Wang, T., Hu, F., Lamb, R. A., Pinto, L. H., Hong, M., Klein, M. L., and DeGrado, W. F. (2011) Molecular Dynamics Simulation Directed Rational Design of Inhibitors Targeting Drug-Resistant Mutants of Influenza A Virus M2. *J. Am. Chem. Soc. 133*, 12834−12841.
(54) Leonov, H., Astrahan, P., Krugliak, M., and Arkin, I. T. (2011) How Do Aminoadamantanes Block the Influenza M2 Channel, and How Does Resistance Develop? *J. Am. Chem. Soc. 133*, 9903−9911.